Electronic Supplementary Material (ESI) for Sustainable Energy & Fuels.

Supporting information

Design of composite cathode and graphene coated separator for stable room-temperature aluminum-sulfur battery

Xiao Zheng, Ruixian Tang, Yu Zhang, Lei Ma, Xiaoyu Wang, Yanru Dong, Guolong Kong, Liangming Wei*

Key Laboratory for Thin Film and Microfabrication Technology of the Ministry of Education, Department of Microelectronics and Nanoscience, School of Electronics Information and Electrical Engineering, Shanghai Jiao Tong University, Dongchuan Road No. 800, Shanghai 200240, China

Table S1. Comparison of the electrochemical performance of S/host composite in this work with other cathode materials reported for aluminum batteries.

Cathode materials	**Initial capacity (mA h g^{-1})**	**Final capacity (mA h g^{-1})**	**Rate (mA g^{-1})**	**Electrolyte (molar ratio)**	**Ref.**
S/host composite	680	1017(38th)	50	$AlCl_3$:[EMIm]Cl	This
	724	198(300th)	100	(1.3:1)	work
	555	218(700th)	200		
polypyrrole	70	51(100th)	20	$AlCl_3$:[EMIm]Cl	[1]
polythiophene	85	73(100th)	16	(1.5:1)	
Poly(nitropyrene-co-pyrene)	162	94(1000th)	200	$AlCl_3$:[EMIm]Cl (1.3:1)	[2]
PVP-I_2	150	189(35th)	42.2	$AlCl_3$:[EMIm]Cl (1.3:1)	[3]
ACC/PVPI	100	180(150th)	42.2	$AlCl_3$:[EMIm]Cl (1.3:1)	[4]
Se nanowires	218	178(50th)	100	$AlCl_3$:[EMIm]Cl (1.1:1)	[5]
$CoSe_2$/C-ND@rGO	326	143(500th)	1000	$AlCl_3$:[EMIm]Cl (1.3:1)	[6]
Te	913	550(20th)	20	$AlCl_3$:[EMIm]Cl	[7]
	400	150(1000th)	500	(1.3:1)	
TeNW/rGO	734	490(100th)	1000	$AlCl_3$:[EMIm]Cl (1.3:1)	[8]

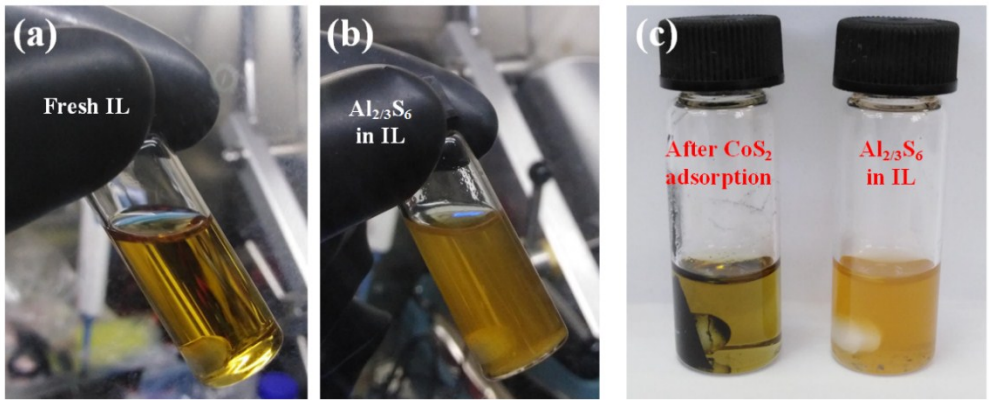

Figure S1. Photographs of a) fresh IL electrolyte, and b) ionic liquid containing $Al_{2/3}S_6$. c) Visualized adsorption of $Al_{2/3}S_6$ on pristine CoS_2.

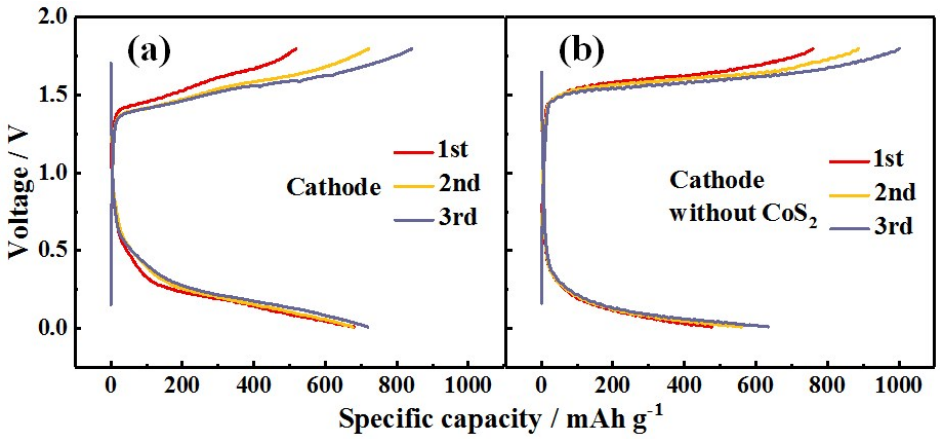

Figure S2. Galvanostatic discharge/charge curves of the batteries with a) cathode+rGO-separator, b) cathode without CoS_2+rGO-separator under a current density of 50 mA g^{-1}.

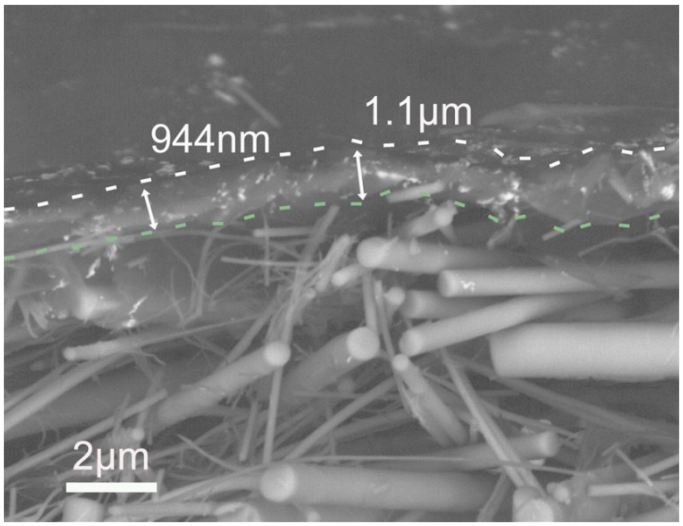

Figure S3. The cross-sectional SEM image of the rGO-separator.

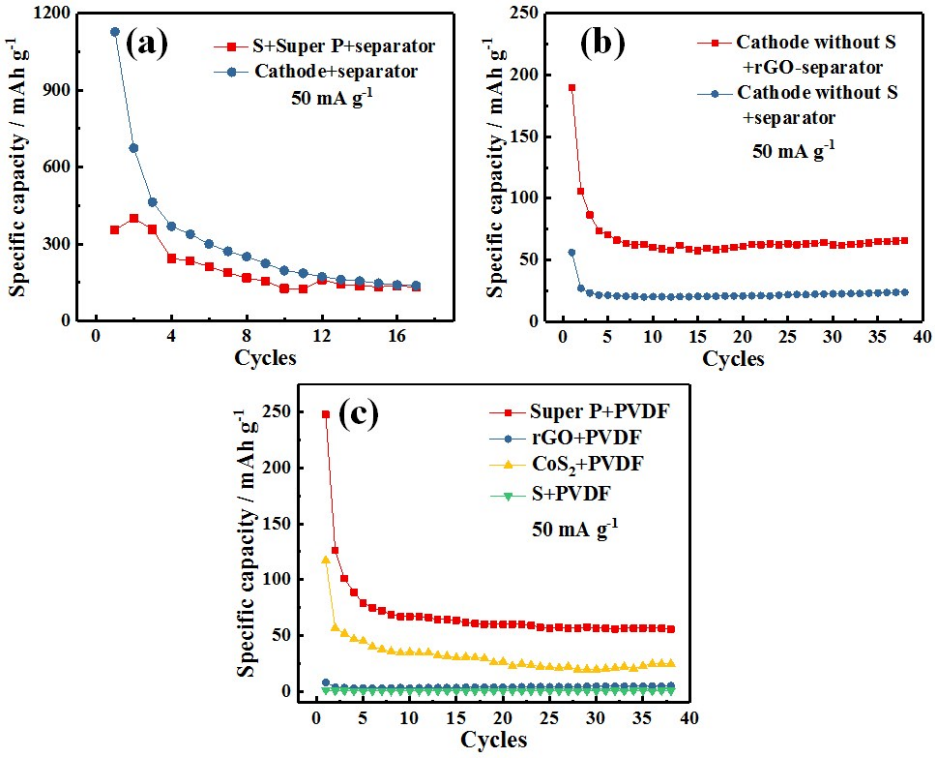

Figure S4. a) Cycling performance of the batteries with S/host cathode+separator and S+Super P+separator. b) Cycling performance of the cathode without S with rGO coated separator and uncoated separator. c) Cycling performance of four individual components of the S/host cathode (i.e., Super P, rGO, CoS_2, and S).

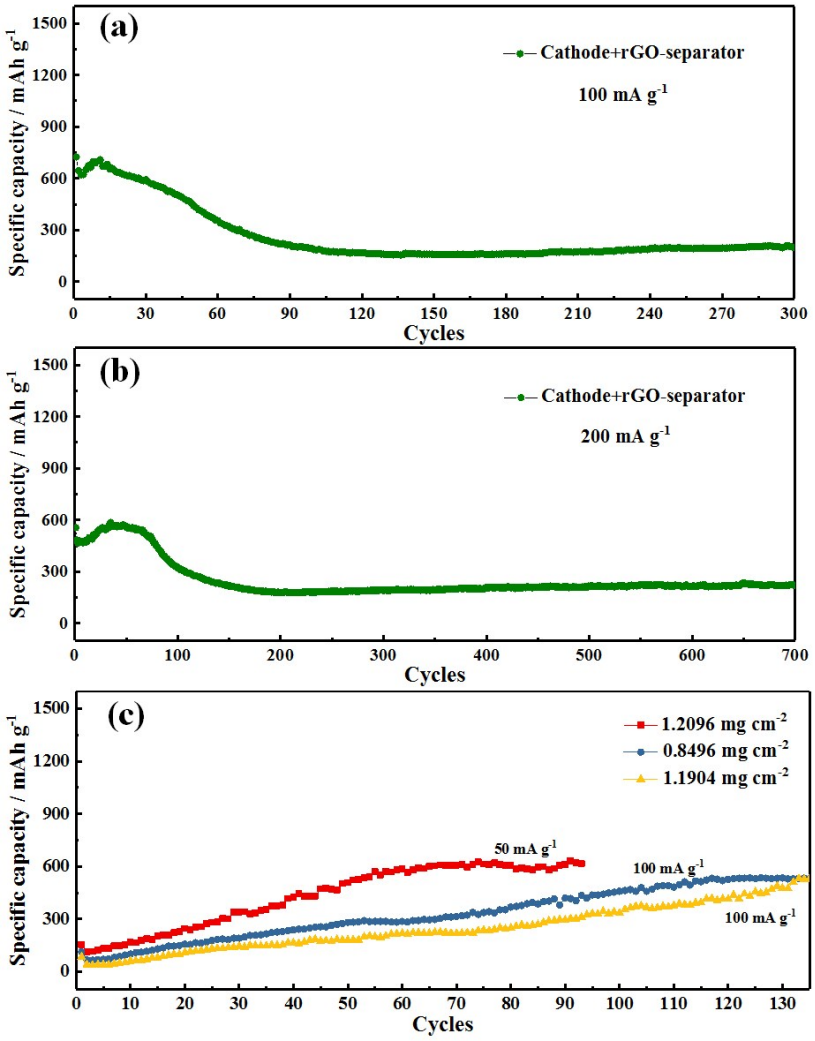

Figure S5. a) Cycling performance of the battery with cathode+rGO-separator at 100 mA g^{-1} for 300 cycles. b) Cycle performance of the battery with cathode+rGO-separator at 200 mA g^{-1} for 700 cycles. c) The cycling stability of composite cathodes with high sulfur loading at 50 and 100 mA g^{-1}.

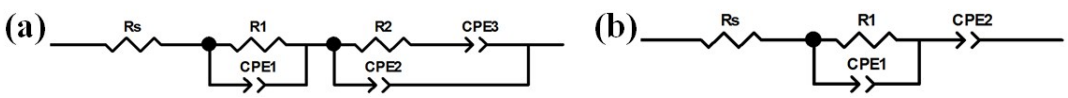

Figure S6. Equivalent circuit model of a) the batteries with cathode+rGO-separator and cathode without S, b) the batteries with cathode+separator.

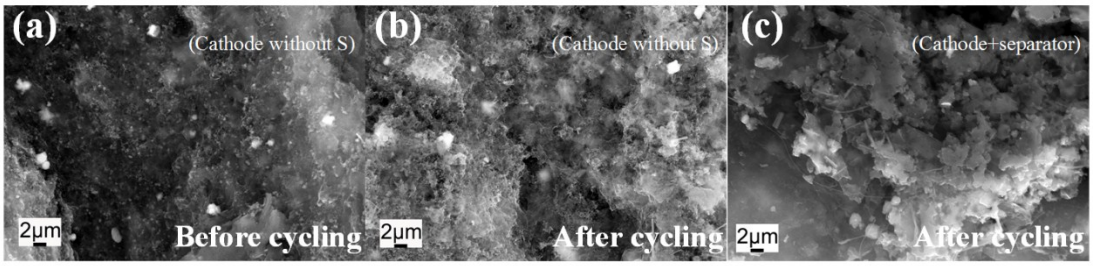

Figure S7. SEM images of a) cathode without S before cycling, b) cathode without S after cycling, c) S/host cathode with uncoated separator after cycling. For a, b) the corresponding separator is rGO-separator.

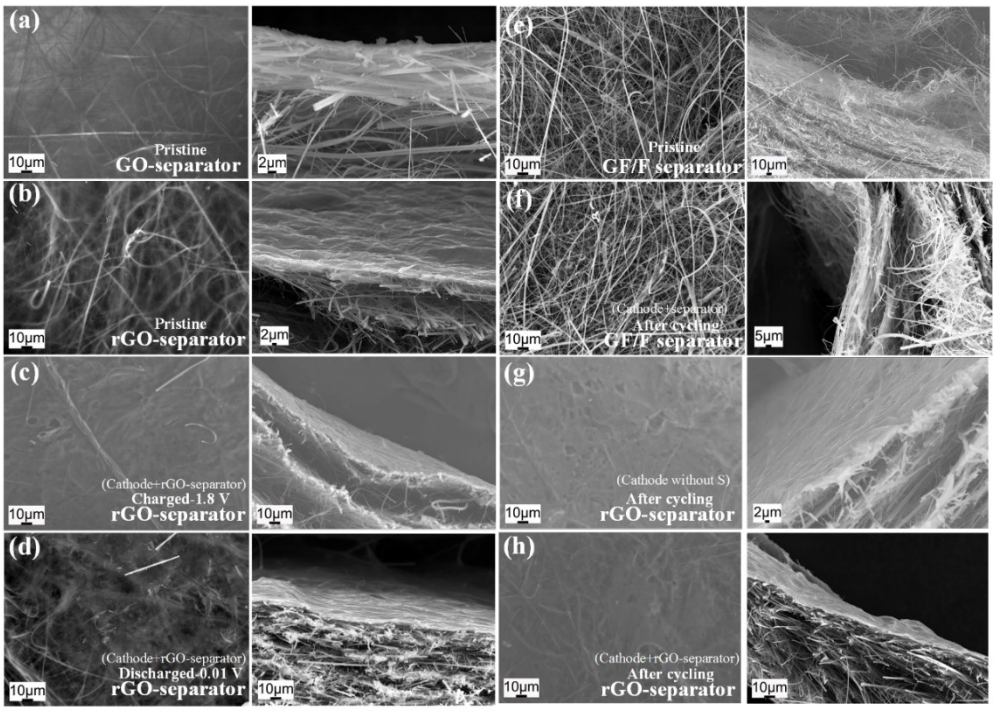

Figure S8. The surface and cross-sectional SEM images of various separators. a) pristine GO-separator, b) pristine rGO-separator, c) rGO-separator from battery charged-1.8 V, d) rGO-separator from battery discharged-0.01 V, e) pristine GF/F separator, f) uncoated separator from battery after cycling, g) rGO-separator from battery after cycling, h) rGO-separator from battery after cycling, for c, d, f, h) the corresponding cathode is S/host cathode, for g) the corresponding cathode is sulfur free.

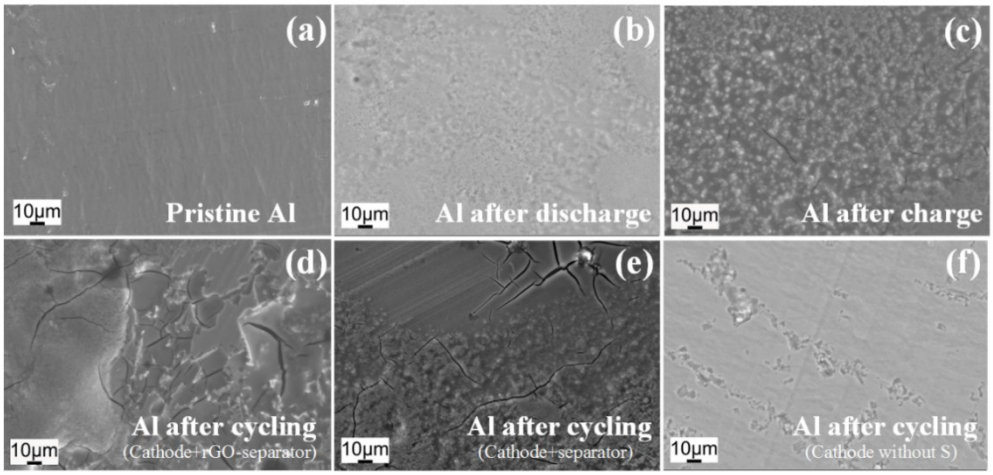

Figure S9. SEM images of a) pristine Al anode, b) Al anode from cathode+rGO-separator discharged-0.01 V, c) Al anode from cathode+rGO-separator charged-1.8 V, d) Al anode from cathode+rGO-separator after cycling, e) Al anode from cathode+separator after cycling and f) Al anode from cathode without S after cycling.

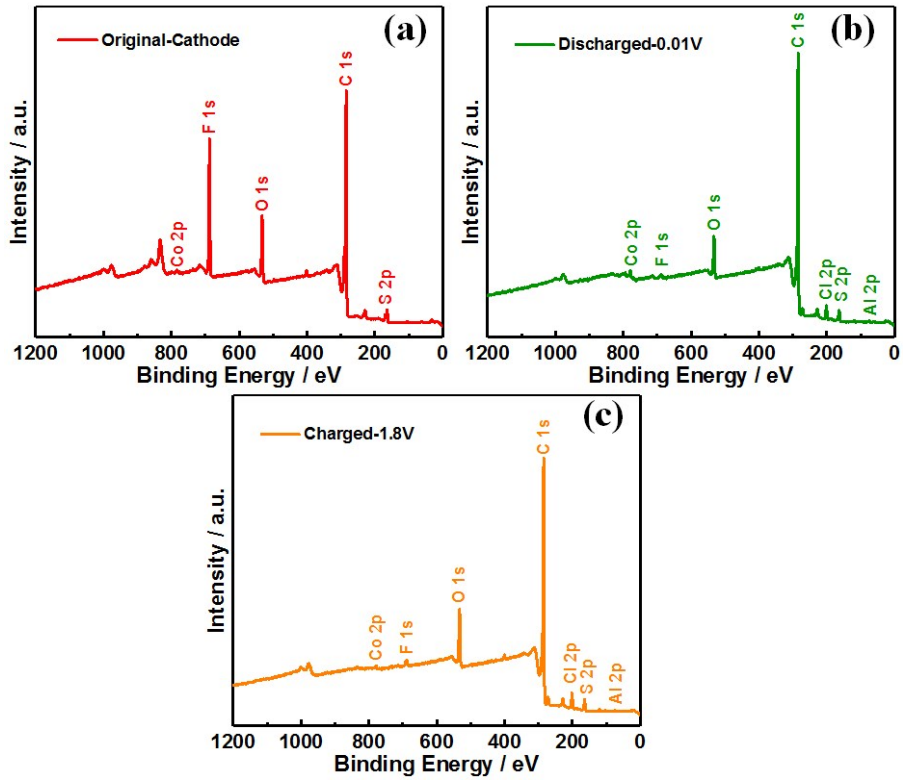

Figure S10. XPS survey spectra of the S/host cathodes in different states: a) original

cathode, b) discharged to 0.01 V, c) charged to 1.8 V.

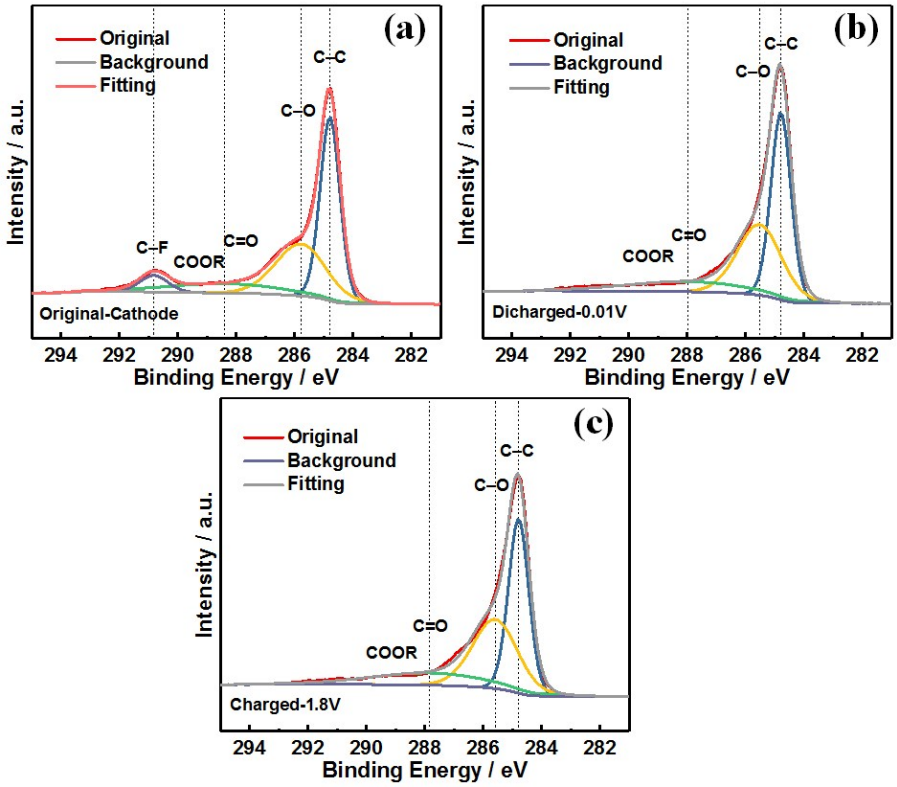

Figure S11. XPS C 1s spectra of the S/host cathodes in different states: a) original cathode, b) discharged to 0.01 V, c) charged to 1.8 V.

It can be seen that the C 1s spectra show strong C–C peak, prominent C–O peak, and weak C=O and O–C=O peaks.

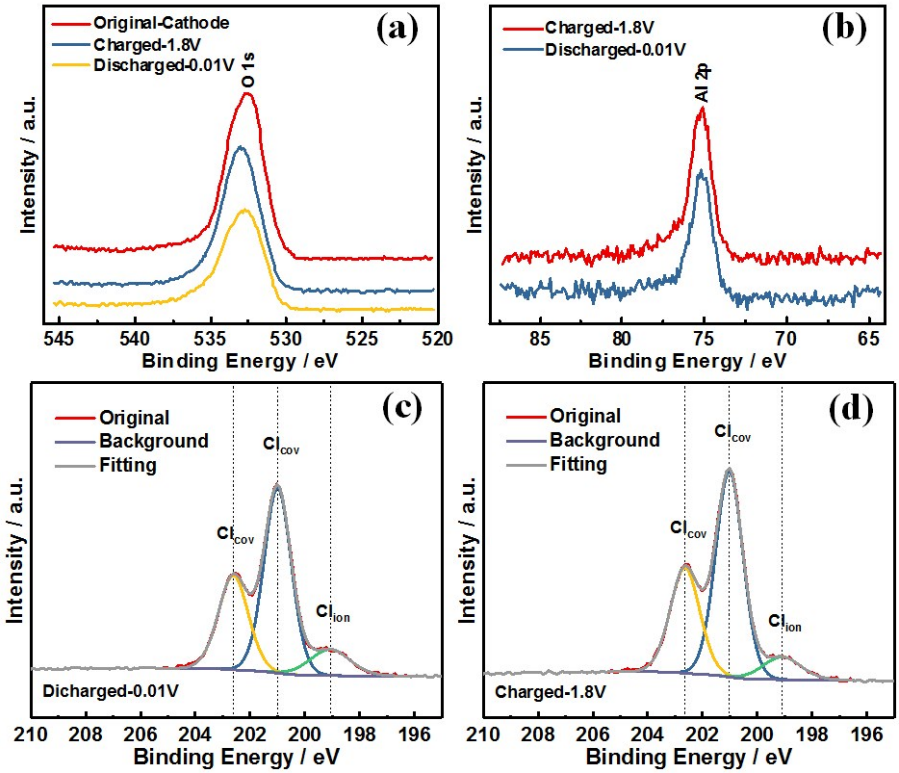

Figure S12. a) XPS O 1s spectra of the S/host cathodes in different states. b) XPS Al 2p spectra of the S/host cathodes in discharged or charged state. XPS Cl 2p spectra of the S/host cathodes in different states: c) discharged to 0.01 V, d) charged to 1.8 V.

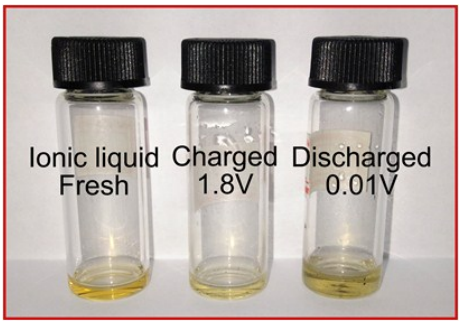

Figure S13. Photograph of [EMIm]Cl-$AlCl_3$ ionic liquid electrolytes in different states.

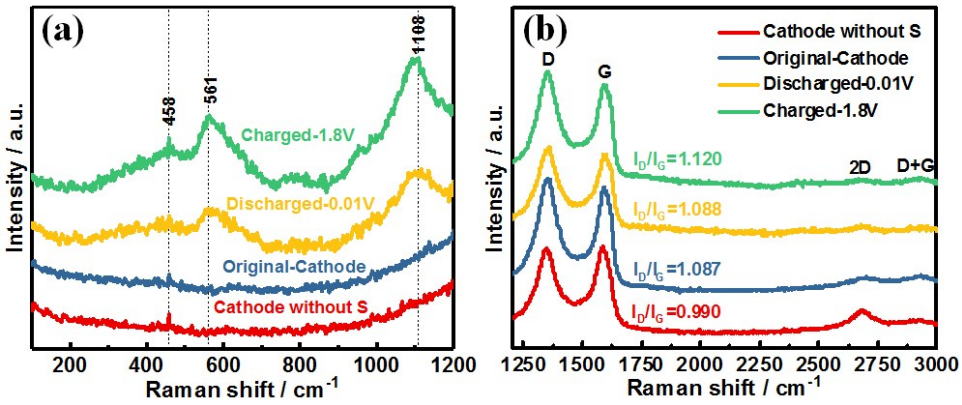

Figure S14. a, b) Raman spectra of S/host cathodes in different states and the cathode without S.

As displayed in Figure S14a, a small peak at 458 cm^{-1} is observed for the original cathode and the cathode without S. As for the cathode in the fully charged or discharged state, in addition to the peak at 458 cm^{-1} with increased intensity, two new broad peaks (561 and 1108 cm^{-1}) appear. These probably attribute to the polysulfides and sulfide combining with residual IL electrolyte generated from the electrochemical conversion reaction during charge and discharge. Raman spectra of the rGO matrix, as displayed in Figure S14b, exhibit broad D-band, G-band, and very weak 2D peak, D + G peak. It can be found that the value of I_D/I_G changes due to the occurring of defect position when the battery is charged or discharged.[9] But the Raman shift remains almost unchanged, it can be concluded that the main role of rGO is the host material, but it takes little part in the reactions.

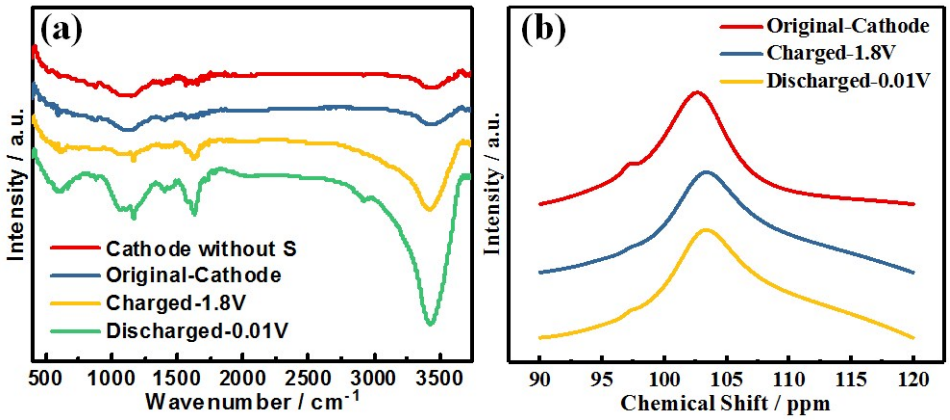

Figure S15. a) FTIR spectra of S/host cathodes in different states and the cathode without S. b) ^{27}Al NMR spectra of S/host cathodes in di□erent states dissolved in $AlCl_3$/[EMIm]Cl IL electrolyte.

Figure S15a shows FTIR spectra of the cathodes in different states and the cathode without S. Two main peaks at 3436 cm^{-1} and 1144 cm^{-1}, which are attributed to ν O–H and ν C–O, are detected in the cathode without S. The original cathode also shows two peaks with ν O–H remaining unchanged while ν C–O shifting to 1116 cm^{-1} after S puts in. When the cathode is fully charged, a new peak which attributed to δ C=C appears at 1618 cm^{-1}, while ν O–H shifting to 3424 cm^{-1} and ν C–O shifting to 1168 cm^{-1} with a relative higher intensity. After fully discharged, ν O–H, δ C=C, ν C–O shift to 3432, 1630, 1167 cm^{-1} with a relative higher intensity respectively. Such phenomenon is ascribed to the electrochemical reaction of the cathode with IL electrolytes.

As shown in Fig. S15b, the original cathode (dissolved in IL electrolyte) shows one broad peak at 103.24 ppm with a small shoulder at 97.23 ppm, which can be assigned to $AlCl_4^-$ and $Al_2Cl_7^-$ species, respectively. These two three-coordinated Al species are from the IL electrolyte. For the fully charged and discharged cathode, a broad peak was also observed, but the small peak on the shoulder was relatively smaller.

References

1. N. S. Hudak, *J. Phys. Chem. C*, 2014, **118**, 5203-5215.
2. M. Walter, K. V. Kravchyk, C. Bofer, R. Widmer and M. V. Kovalenko, *Adv. Mater.*, 2018, **30**, e1705644.
3. H. Tian, S. Zhang, Z. Meng, W. He and W.-Q. Han, *ACS Energy Lett.*, 2017, **2**, 1170-1176.
4. S. Zhang, X. Tan, Z. Meng, H. Tian, F. Xu and W.-Q. Han, *J. Mater. Chem. A*, 2018, **6**, 9984-9996.
5. X. Huang, Y. Liu, C. Liu, J. Zhang, O. Noonan and C. Yu, *Chem. Sci.*, 2018, **9**, 5178-5182.
6. T. Cai, L. Zhao, H. Hu, T. Li, X. Li, S. Guo, Y. Li, Q. Xue, W. Xing, Z. Yan and L. Wang, *Energy Environ. Sci.*, 2018, **11**, 2341-2347.
7. H. Jiao, D. Tian, S. Li, C. Fu and S. Jiao, *ACS Appl. Energy Mater.*, 2018, **1**, 4924-4930.
8. X. Zhang, S. Jiao, J. Tu, W.-L. Song, X. Xiao, S. Li, M. Wang, H. Lei, D. Tian, H. Chen and D. Fang, *Energy Environ. Sci.*, 2019, **12**, 1918-1927.
9. S. Wang, Z. Yu, J. Tu, J. Wang, D. Tian, Y. Liu and S. Jiao, *Adv. Energy Mater.*, 2016, **6**, 1600137.